AD-A157 225 EQUILIBRIUM AND STABILITY OF THE SOLENOIDAL LENS BETATRON(U) MISSION RESEARCH CORP ALBUQUERQUE NM T P HUGHES ET AL. JUN 85 AMRC-N-308 N00014-84-C-0078 1/1

UNCLASSIFIED F/G 20/7 NL

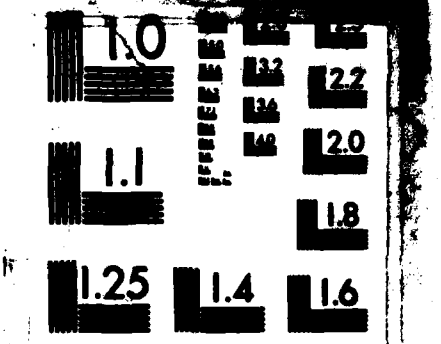

AMRC-N-308
Copy 95

EQUILIBRIUM AND STABILITY OF THE SOLENOIDAL LENS BETATRON

Thomas P. Hughes
Brendan B. Godfrey

THE NEGATIVE MASS INSTABILITY IN HIGH CURRENT MODIFIED BETATRONS AT LOW ENERGIES

Brendan B. Godfrey
Thomas P. Hughes

June 1985

Presented at: 1985 Particle Accelerator Conference
Vancouver, British Columbia, Canada

Prepared for: Office of Naval Research
Physical Sciences Division
800 North Quincy Street
Arlington, Virginia 22217

Under Contract: N00014-84-C-0078

Prepared by: MISSION RESEARCH CORPORATION
1720 Randolph Road, S.E.
Albuquerque, New Mexico 87106

EQUILIBRIUM AND STABILITY PROPERTIES OF THE SOLENOIDAL LENS BETATRON

Thomas P. Hughes and Brendan B. Godfrey
Mission Research Corporation, 1720 Randolph Road, S.E.
Albuquerque, New Mexico 87106

Summary

The solenoidal lens betatron[1] uses a series of solenoidal lenses arranged around a race-track shaped drift-tube to provide strong transverse focusing for a high-current electron ring. Equilibrium behavior of the circulating beam is examined for parameters close to those of the University of New Mexico machine currently under construction. The tolerance of the beam to mismatches in the toroidal and vertical fields is evaluated analytically and using a particle simulation code. The linear and nonlinear development of the negative-mass instability in the device is also studied. Stability behavior comparable to that in a conventional betatron (i.e., one with no toroidal magnetic field) is found. Growth rates are compared to those obtained from an analytic model.

Equilibrium Properties

In order to confine and accelerate high currents in a betatron, the conventional weak focusing must be supplemented. In the solenoidal lens betatron (SLB)[1] this is accomplished through the use of periodic solenoidal lenses, as shown in Fig. 1. The SLB thus differs from the "modified" betatron,[2] for example, which uses a uniform toroidal field. For a matched equilibrium, the beam in the SLB reverses its poloidal rotation at each lens, so that the net poloidal rotation is zero. This requires that the beam be injected from a cathode which is shielded from magnetic flux, so that the beam produced has no canonical poloidal angular momentum. In the region between lenses, the beam rotates at the Larmor frequency, i.e., $\Omega_\theta/2\gamma$, where Ω_θ is the nonrelativistic cyclotron frequency in the solenoidal field, and γ is the relativistic factor. If the beam emittance is negligible, then force-balance requires

$$\frac{1}{2} - n_s + \rho^2/4 = 0 \qquad (1)$$

where $n_s = 2\nu R^2/\gamma^3\beta^2a^2$, is the self-field index, ν is Budker's parameter (beam current divided by 17 kA), R and a are major and minor beam radii, respectively, β is the beam velocity normalized to c, ρ is the ratio B_θ/B_z, where B_z is the vertical betatron field, and B_θ is the solenoidal (toroidal) field between the lenses. We have assumed that the vertical field index is 1/2. From Eq. (1), we can compute the solenoidal field needed for a matched beam, given the other quantities. Sample parameters for initial experiments at the University of New Mexico (UNM) are: R = 1 m, a = 2 cm, γ = 3, $\nu = 5.9\times10^{-3}$ (100 Amps). From these, we compute that B_θ = 80 Gauss is required. This result is expected to be accurate in the limit where the thickness of the magnetic cusps is much less than the distance between them. A scenario closer to that envisioned for the UNM device is to have 21 cm long solenoids spaced 10.5 cm apart. There are thus 20 solenoids evenly spaced around the 1 m major radius torus. We model the magnetic fields by using the exact, numerically computed values for finite length straight solenoids. One "cell" of the periodic field is shown in Fig. 2. Simulations of beam behavior in this device are carried out using the electromagnetic particle code IVORY.[3] We find that to minimize the envelope fluctuations, the field in the middle of each solenoid must be about 100 Gauss. The discrepancy between this and the analytic result is presumably due to the thickness of the cusps, which lowers the average field value.

*Work supported by the Office of Naval Research.

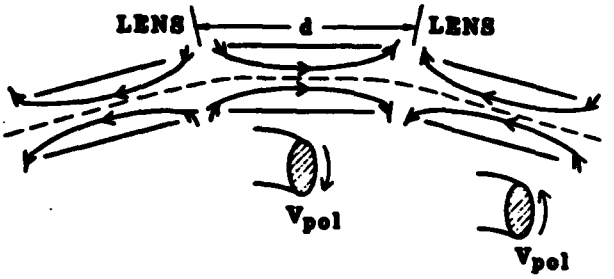

Figure 1. Section of Solenoidal Lens Betatron. The poloidal velocity V_{pol} reverses from one solenoid to the next.

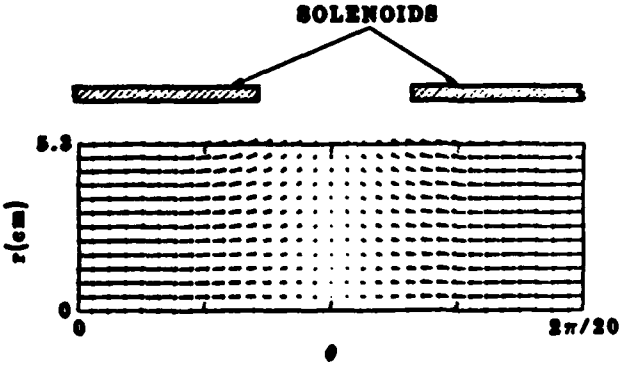

Figure 2. Vector plot of one-half period of toroidal field, showing location of solenoidal windings.

Mismatch in Solenoidal Field

To check the tolerance of the beam to mismatch in the solenoidal field, we run two cases in which the value of B_θ is doubled and halved respectively. In each case, we ensure that the beam has zero canonical poloidal angular momentum. The resulting envelope oscillation amplitudes are shown in Fig. 3. The beam oscillates between radii of 2 cm and 0.5 cm for B_θ = 200 Gauss, and between 2 cm and 3 cm for B_θ = 50 Gauss. Experimentally, it should not prove difficult to avoid these large mismatches.

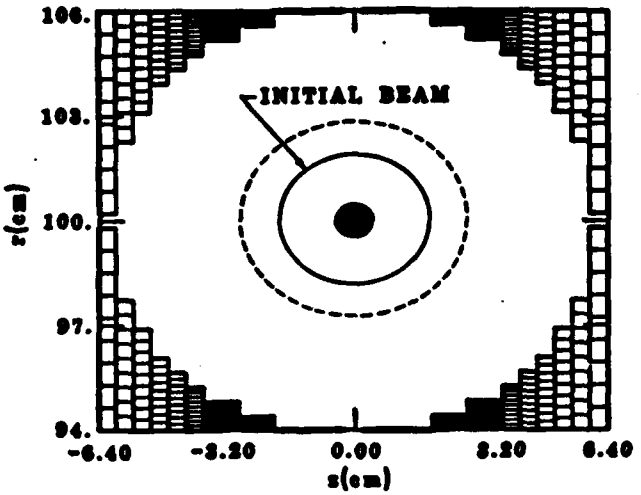

Figure 3. Amplitude of envelope oscillations for (i) B_0 = 200 Gauss (inner bullet), (ii) B_0 = 50 Gauss (dashed outer line).

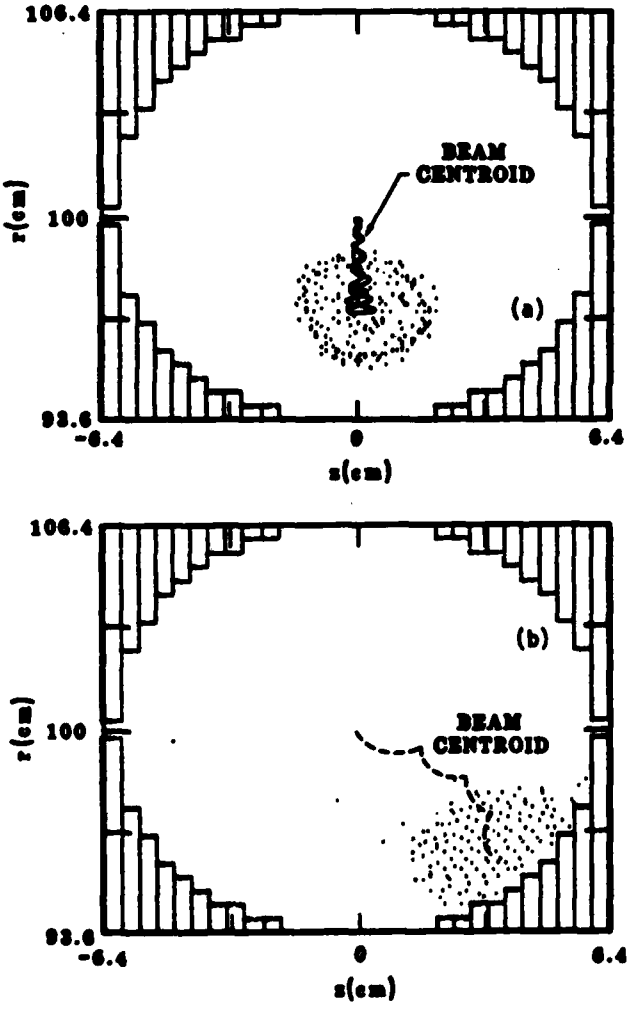

Figure 4. Effect of 1.5% vertical field mismatch in (a) SLB, (b) modified betatron.

Mismatch In Vertical Field

For a given value of the vertical field B_z, the matched major radius of the beam is $r = \beta\gamma c/\Omega_z$, where r measures the distance from the major axis of the torus. Transverse oscillations about this radius are determined from the equation,

$$\Delta\ddot{r} + \Delta r\left(\frac{1}{2} - n_s\frac{a^2}{b^2} + p^2/4\right)\Omega_z^2/\gamma^2 = \frac{\Delta B_z c^2}{B_z R} \qquad (2)$$

where b is the minor radius of the drift-tube, and ΔB_z is the mismatch in the vertical field. This equation is valid in the thin-lens limit, in which the solenoidal lenses act as a continuous radial focusing force on the beam. Equation (2) predicts a momentum compaction factor $\alpha = (1/2 - n_s a^2/b^2 + p^2/4)^{-1}$. The effect of a 1.5% vertical field mismatch is shown in the particle simulation in Fig. 4, in which we assume the sample UMM beam parameters given above, and B_0 = 100 Gauss. For these parameters, $\alpha = 1$, so that the beam oscillates about an equilibrium major radius of 98.5 cm. For comparison, the momentum compaction factor of the weak-focusing modified betatron is $\alpha = (1/2 - n_s a^2/b^2)^{-1} = 2.5$. In this case a 1.5% mismatch in the vertical field gives the beam an average major radius of 96 cm. As seen in Fig. 4, the oscillation about this position brings the beam in contact with the wall. Even with the improved mismatch behavior of the SLB, however, keeping the vertical field matched to the beam energy to within a few percent will require delicate tuning of the experiment.

Stability Properties

A circulating high-current electron ring may be subject to several types of instabilities, including negative-mass, resistive wall, and, in the case of the SLB, which has accelerating gaps, the beam break-up instability. In addition, single particle orbital resonances may affect beam quality. Here, we concentrate on the negative-mass instability, since it is potentially the most serious collective instability.[3] An analytic, high-current theory of this and some closely related instabilities is described in a companion paper.[4] The theory is directly applicable only to devices in which the toroidal coordinate is ignorable in the equilibrium, such as the modified betatron. However, we use the theory here as a guide in discussing the stability of the SLB. Our numerical results obtained from 3-D simulations using IVORY are not restricted this respect. However, the number of simulations we can perform, and their length, is small due to computing expenses. We have therefore concentrated on making runs at high currents, where relatively large growth rates are expected.

The first case we look at is a 10 kA, 5.5 MeV beam with a = 2 cm, and R = 1 m. We find that a solenoidal field of 600 Gauss can transport this beam with minimal (<10%) envelope modulation. The solenoidal lenses have the same configuration as in Fig. 2. The beam is given a small initial perturbation, and the growth of $\ell = 20$ fields on the beam is followed. The justifications for following just one mode in the simulations are: a) In the linear regime, mode-coupling should be negligible; b) By following one mode, direct comparison with linear theory predictions for that particular mode are possible; c) Since there are 20 solenoids around the torus, the $\ell = 20$ mode is likely to have a large initial perturbation; d) Computing costs severely limit the number of toroidal modes one can afford to keep. In the simulation just mentioned, we find a rapid linear growth rate of $\Gamma = 1.62\times10^6$ sec^{-1}. The effect of the instability on the beam as it reaches nonlinear levels is shown in Fig. 5. The behavior is similar to the negative-mass behavior that one would expect to see in a

conventional betatron ($B_\theta = 0$).[5] The radial deflection of the beam seen in Fig. 5(a) is accompanied by the toroidal bunching in Fig. 5(b). This behavior leads us to compare the linear growth rate with that obtained from theory[5] for a $B_\theta = 0$ beam. We find that the theoretical growth rate is very close: 1.63×10^8 sec^{-1}. In Fig. 6, we compare results for the SLB at other energies with the theory. For comparison, results for the same beam in a modified betatron with a 1 kG toroidal field are shown. In Fig. 7, the same curves are plotted for a 1 kA beam with a = 1 cm. For these parameters, we have just one simulation result, at 5.5 MeV, and the growth rate is again seen to be close to the $B_\theta = 0$ result.

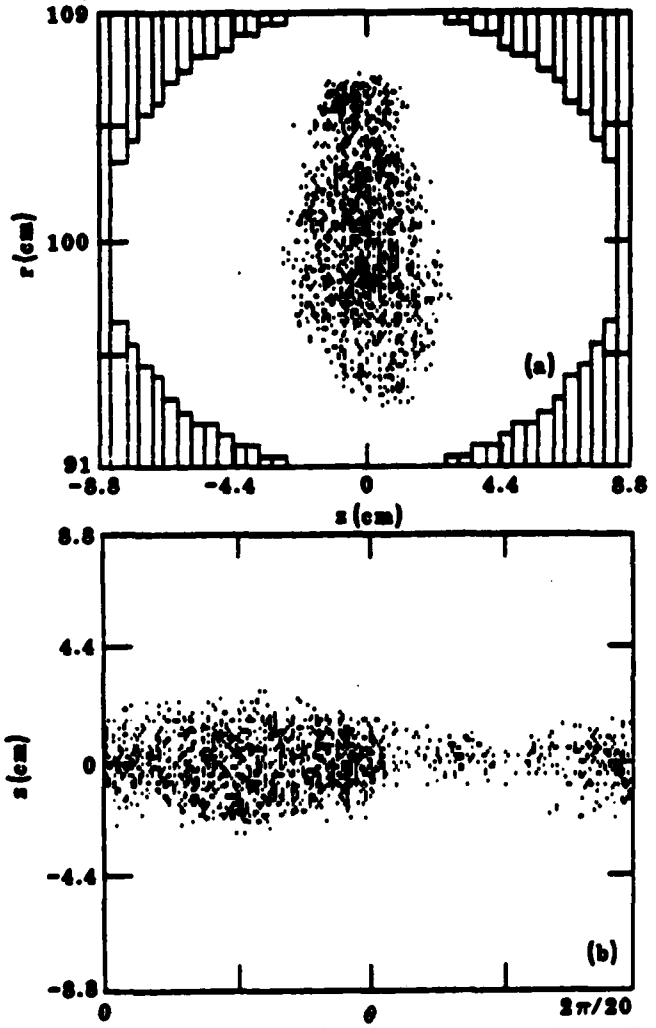

Figure 5. Effect of $\ell = 20$ negative-mass mode on 10 kA SLB beam. Particles at all θ-positions are plotted in (a).

We must note that the results in Fig. 6 for the case $B_\theta = 0$ are somewhat artificial when $\gamma < 18$. In this regime, weak focusing alone is insufficient to hold the beam together. The analytic model from which the growth rates are obtained uses a rigid disk model of the beam, and so ignores the force balance required within the beam. It is tempting to conclude from the results in Fig. 6 that in the SLB, the strong focusing provides the necessary forces the hold the beam equilibrium together, but that the negative-mass instabilities on the beam behave as if the toroidal field were zero. Further numerical and analytic work will be performed to check this conclusion.

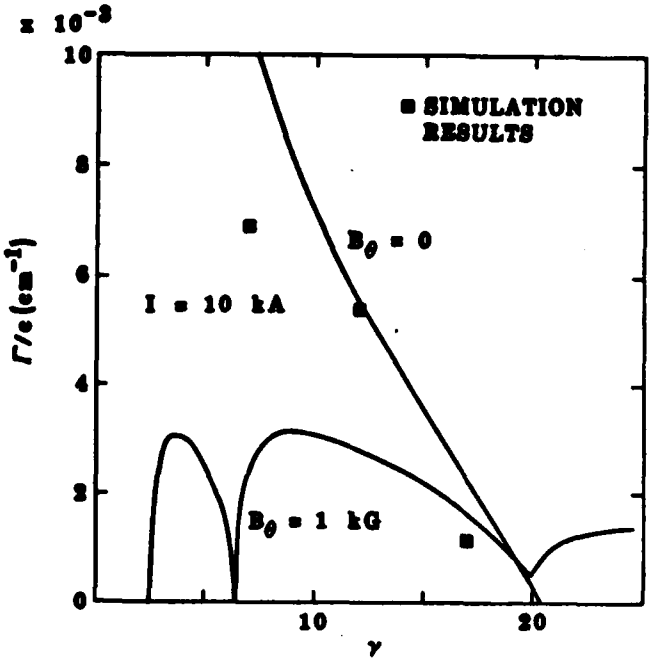

Figure 6. Growth rates of $\ell = 20$ mode versus energy. Simulation results for SLB, and analytic results for conventional ($B_\theta = 0$) and modified ($B_\theta = 1$ kG) betatronsare shown.

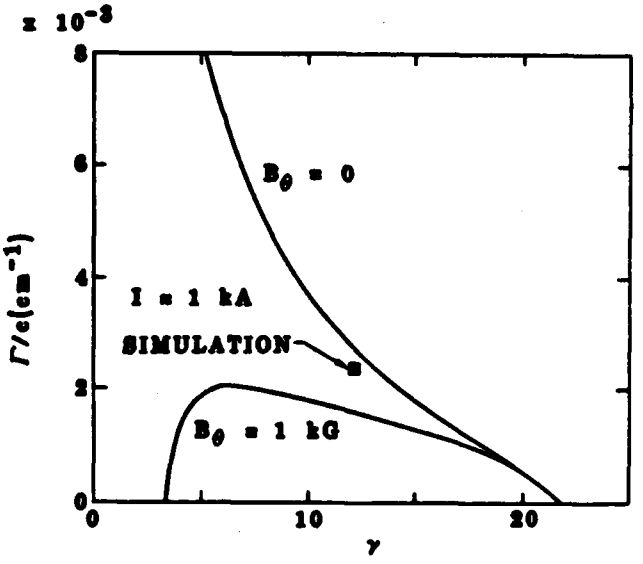

Figure 7. Growth rates of $\ell = 20$ instability for a 1 kA beam with 1 cm radius. Curves have same meaning as in Fig. 6.

References

1. S. Humphries, Jr. and D. M. Woodall, Bull. Am. Phys. Soc. 28, 1054 (1983).
2. P. Sprangle, C. A. Kapetanakos, and S. J. Marsh, Proc. 4th Intl. Conf. on High Power Electron and Ion Beams (Palaiseau, France, 1981).
3. T. P. Hughes, M. M. Campbell, and B. B. Godfrey, AMRC-R-524 (Mission Research Corp., 1983); Phys. Fluids 28, 669 (1985).
4. B. B. Godfrey and T. P. Hughes, this conference.
5. R. W. Landau and V. K. Neil, Phys. Fluids 9, 2412 (1966).

THE NEGATIVE MASS INSTABILITY IN HIGH CURRENT MODIFIED BETATRONS AT LOW ENERGIES

Brendan B. Godfrey and Thomas P. Hughes
Mission Research Corporation, 1720 Randolph Road, S.E.
Albuquerque, New Mexico 87106

Abstract

We have developed a new linearized, rigid-disk model of negative mass instabilities in high current betatrons. Taking the beam and accelerator cavity cross sections to be rectangular permits the electromagnetic fields to be evaluated exactly in toroidal geometry. Growth rates from the model agree well with results of three-dimensional numerical simulations for beams and cavities with rectangular or cylindrical cross sections. Generally, negative mass instability growth rates are greatest for beam energies within a factor of two of the so-called transition energy and in that energy regime scale inversely with the square root of the toroidal magnetic field strength. At much higher energies, growth rates are nearly independent of toroidal field strength. Growth rates increase with beam current and toroidal mode number, but the scaling laws tend to be complicated by competition between capacitive and inductive components of the toroidal cavity fields.

Introduction and Summary

Betatrons employing toroidal magnetic fields [1,2], possibly augmented by strong-focusing fields [3-6], seem capable of accelerating moderate current electron beams to high energies. Beam stability, along with injection and extraction, is an important issue not yet completely resolved. Among instabilities, the negative mass mode probably is most serious, as it has been for other electron ring devices [7]. In this paper we present an improved linear model of the negative mass instability in cold beams, obtain growth rate expressions, and compare these findings with the results of three-dimensional computer simulations.

As in earlier treatments, we approximate the beam as a string of rigid disks [8,9], because the instability has the form of a uniform transverse beam displacement. The electromagnetic fields, however, are evaluated exactly, although for a beam and cavity of rectangular minor cross section in order to simplify the analysis. Accurately determining the fields is critical because of delicate cancellations among terms in the resulting dispersion relation [9]. Simulations (with IVORY [10]) suggest that the choice of cross section, while artificial, does not appreciably alter the character of our results.

The most important outcome of the new model is its much improved agreement with simulation data, which enhances our confidence in predictions of experimental behavior.

Interestingly, the model also shows that inductive electric fields can dominate electrostatic fields at large toroidal mode numbers, giving rise to reduced instability growth rates and, for a few modes, a stability window. The window can be shifted to low toroidal modes by moving the electron beam toward the inner wall of the cavity. The analogous situation for a fast rotating e-layer immersed in a strong azimuthal magnetic field is treated in Ref. [11] to check the betatron results and to provide more insight into the underlying physics.

Analytical Results

We consider a rectangular cross section beam and cavity with dimensions as shown in Fig. 1. The beam may be located radially anywhere in the cavity but must be centered axially for a static equilibrium.

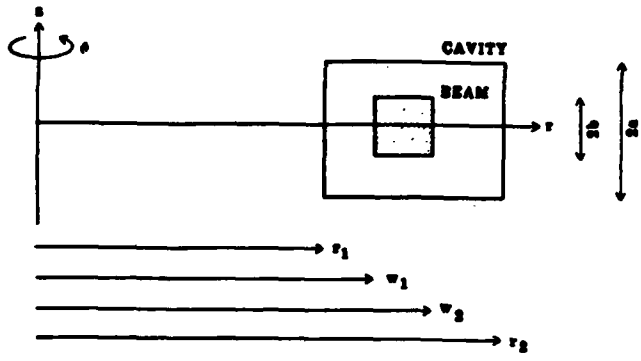

Figure 1. Beam and toroidal cavity cross sections.

Treating the beam as a set of rigid disks and evaluating its fields by a Green's function approach leads to a dispersion relation of the usual form

$$(\Omega^2 - \omega_z^2)(\Omega^2 - \omega_r^2 - \frac{\chi}{\Omega^2 - \varepsilon}) - \Omega^2 \frac{B_\theta^2}{\gamma^2} = 0 \quad (1)$$

where $\Omega = \omega - l\omega_0$, $\omega_0 = V_\theta/R$, $R = (w_1+w_2)/2$, and B_θ is the polodial cyclotron frequency. Expressions for the axial and radial bounce frequencies, the longitudinal dielectric function, and the coupling function are extremely complex but may be approximated as, respectively, [10]

$$\omega_z^2 = n\omega_0^2 - g_1 \frac{2\nu}{\gamma^3 b^2} \quad (2)$$

$$\omega_r^2 = (1-n)\omega_0^2 - g_2 \frac{2\nu}{\gamma^3 b^2} \quad (3)$$

$$\varepsilon = \frac{\nu}{\gamma^3}\left(g_3 \frac{l^2}{R^2} - g_4 \omega^2\right) \quad (4)$$

$$\chi = \left(\gamma\omega_0\Omega + \frac{\nu}{\gamma^2}\frac{l^2}{R^2} g_5\right)^2 - \gamma^2\omega_0^2(\Omega^2 - \varepsilon) \quad (5)$$

Here, n is the betatron field index, ν is the beam current normalized to 17 kA, γ is its relativistic energy, and g_i are geometrical factors of order unity. Much of the physics is, of course, contained in those factors, the latter three of which must be accurately evaluated numerically due to cancellations between the inductive and electrostatic components of Eq. (4) and (5).

Approximate analytical solutions to Eqs. (1)-(5) can be obtained at energies above the transition energy, i. e., for the right side of Eq. (2) positive. See Table 1. It is often true that

$$x = \frac{\gamma^2}{R^2}\,\epsilon_0 \qquad (6)$$

where ϵ_0 is ϵ evaluated at $\Omega = 0$. When this is so, Cases 1A and 1C of Table 1 correspond to the usual negative mass growth rate expressions for a low current betatron without [12] and with [13] a toroidal magnetic field. The poloidal bounce frequency used in the table is defined as

$$\omega_B^2 = \omega_r^2\,\omega_z^2/\left(B_\theta^2/\gamma^2\right) \qquad (7)$$

TABLE 1. APPROXIMATE DISPERSION RELATION SOLUTIONS

B_θ	x	$\Omega^2 =$	CASE
$\omega_B^2 >> \omega_\theta^2$	$\lvert x\rvert << \left(\frac{\omega_r^2}{2}\right)^2$	$\omega_r^2, -\frac{x}{\omega_r^2}$	1A
	$\lvert x\rvert >> \left(\frac{\omega_r^2}{2}\right)^2$	$\pm x^{1/2}$	2A
$\omega_\theta^2 >> \omega_B^2 >> \epsilon$	$\lvert x\rvert << \left(\frac{\omega_r\omega_B}{2}\right)^2$	$\omega_B^2, -\frac{x}{\omega_r^2}$	1B
	$\lvert x\rvert >> \left(\frac{\omega_r\omega_B}{2}\right)^2$	$\pm\left(x\frac{\omega_B^2}{\omega_r^2}\right)^{1/2}$	2B
$\epsilon >> \omega_B^2$	$\lvert x\rvert << \left(\frac{\epsilon}{2}\frac{\omega_r}{\omega_B}\right)^2$	$\epsilon, -\frac{x}{\epsilon}\frac{\omega_B^2}{\omega_r^2}$	1C
	$\lvert x\rvert >> \left(\frac{\epsilon}{2}\frac{\omega_r}{\omega_B}\right)^2$	$\pm\left(x\frac{\omega_B^2}{\omega_r^2}\right)^{1/2}$	2C

Numerical Results

We next solve the full dispersion relation, using the methods described in Ref. [10], to illustrate typical instability growth rate scaling with beam current, energy, toroidal field, and mode number. We choose a square beam, b = 1.76 cm, centered in a square cavity, a = 8.8 cm. The major radius is R = 100 cm, and the field index is n = 1/2.

Figures 2 and 3 depict respectively $\ell = 1$ and 20 negative mass instability growth rates for 10 kA and 1 kA beams in a 1 kG guide field. Results for $\ell = 1$ with $\gamma > 10$ agree well with Case 1B of Table 1. The growth rate scales linearly with ℓ and $\sqrt{\nu}$. Note that the growth rates at high energies vary roughly as $\gamma^{-1/2}$ for $\ell = 1$ because g_3 slightly exceeds g_4, and as $\gamma^{-3/2}$ for $\ell = 10$ (not shown) because g_3 and g_4 are for that case equal. For high energies and moderate toroidal magnetic fields,

$$\Gamma = \frac{\ell}{R}\,\frac{1}{1-n}\,\frac{\nu}{\gamma}\left[\left(g_3 - g_4\,\nu_\theta^2\right)\right]^{1/2} \qquad (8)$$

Scaling of growth rates at low energies is not so clean but appears to go as $(\ell/\nu)^{1/2}$.

When $\ell > 11$ the standard negative mass instability is cut off by inductive effects for x negative, i. e. γ greater than

$$\gamma_{co} = \left(1 - g_3/g_4\right)^{-1/2} \qquad (9)$$

The cutoff shown for the 1 kA beam at $\ell = 20$ in Fig. 3 satisfies Eq. (9) well. Note also the first appearance of a second instability branch in a narrow band around $\gamma = 24$ due to resonant coupling of the beam longitudinal and transverse modes. This hybrid mode is much stronger in the 10 kA beam and connects directly to the usual branch of the instability at $\gamma = 18$. For $\ell = 30$ (not shown), $\gamma_{co} = 12$; the hybrid negative mass instability is well developed for both 10 kA and 1 kA, and is accurately represented by Case 2B of the table.

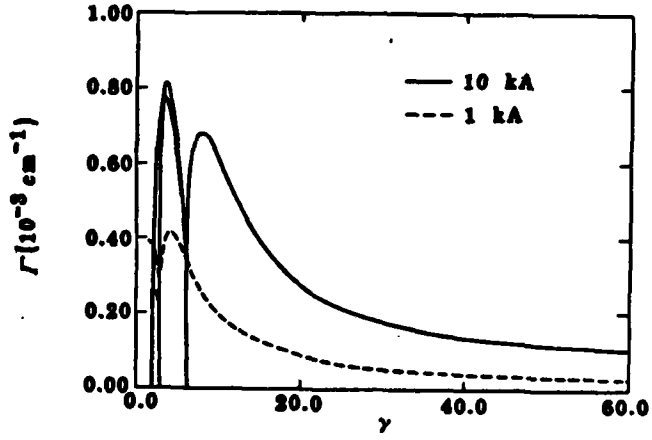

Figure 2. Negative mass $\ell = 1$ growth rates for 10 and 1 kA beams in a 1 kG guide field.

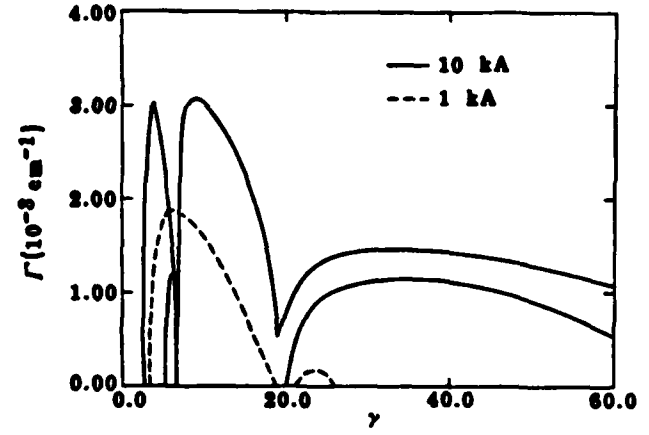

Figure 3. Negative mass $\ell = 20$ growth rates for 10 and 1 kA beams in a 1 kG guide field.

Instability growth rate scaling with B_θ is presented in Fig. 4 and 5 for the 10 kA beam at $\ell = 1$ and 20. Results for 1 kG, 10 kG, and 100 kG guide fields are shown. Corresponding data for 0 kG are not given for $\ell = 1$, and for $\ell = 20$ below γ_{co}, because they are indistinguishable from the 1 kG results at energies for which an equilibrium exists (above about 18 MeV). The 0 kG betatron is stable above γ_{co} for $\ell = 20$. In general, we expect the guide field to have negligible influence on beam stability for low ℓ (e. g., Fig. 4) so long as the poloidal bounce frequency is less than $\sqrt{\epsilon}$. For the present parameters this is true for B_θ less than a few kG at $\gamma = 10$ and a few thousand kG at $\gamma = 50$. Hence, we see a steady drop in the peak of the growth rate curve as B_θ is increased above 1 kG until it reaches Case 1C at 100 kG. Note that growth below the transition energy is eliminated. In contrast, growth rates at the highest energies shown in the plot are little reduced.

Below γ_{co} instability behavior at $\ell = 20$, displayed in Fig. 5, is qualitatively similar to that at $\ell = 1$. Growth rates above the inductive transition energy are expected, based on Table 1, to fall off with magnetic field as $B_0^{-1/2}$ once ω_B somewhat exceeds $\hat{\omega}_\beta$. This happens above a few kG for energies of interest in Fig. 5.

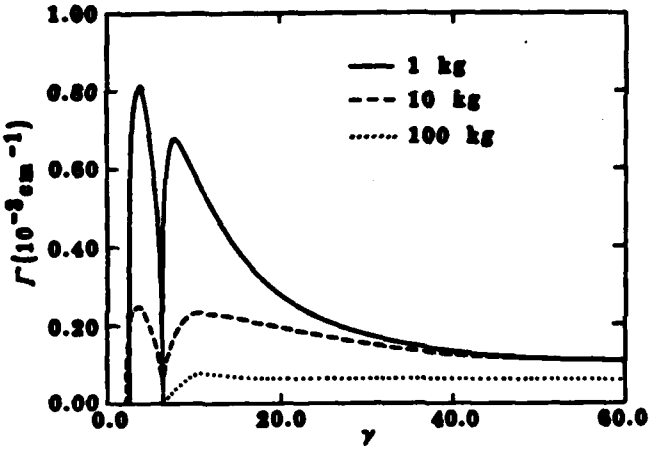

Figure 4. Negative mass $\ell = 1$ growth rates for a 10 kA beam in 1, 10, and 100 kG guide fields.

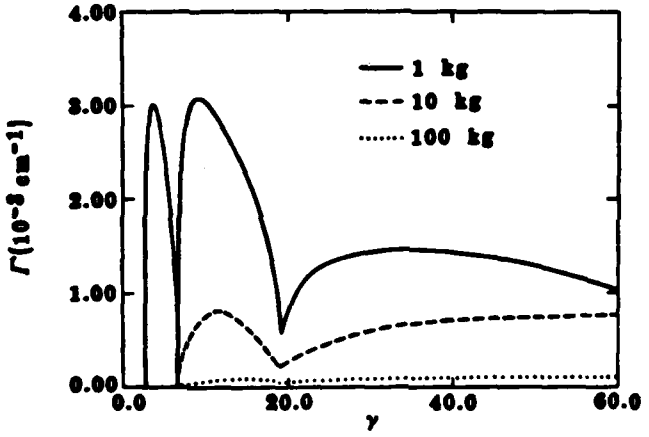

Figure 5. Negative mass $\ell = 20$ growth rates for a 10 kA beam in 1, 10, and 100 kG guide fields.

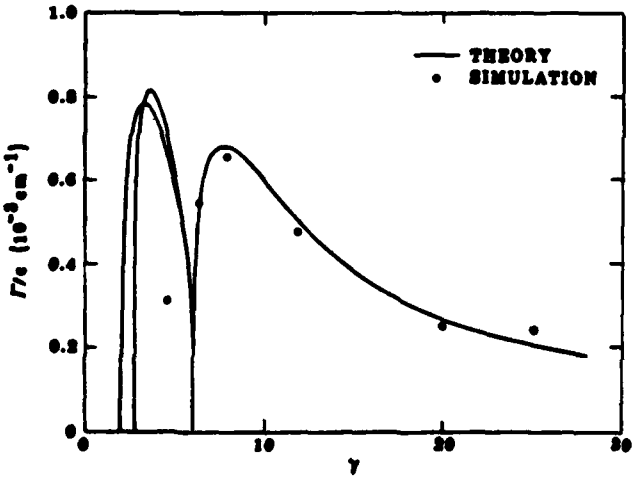

Figure 6. Negative mass $\ell = 1$ growth rates for a 10 kA beam in a 1 kG guide field.

Comparison with Simulations

We conclude this paper with a brief comparison of dispersion relation curves with growth rates determined by the computer simulation code IVORY. The simulation data points were, for the most part, already reported in Ref. [9]. Figure 6 gives $\ell = 1$ results for a 10 kA beam in a 1 kG guide field. Agreement is excellent except for the $\gamma = 5$ data point. The discrepancy probably is due to beam temperature in the simulation. Figure 7 treats the same beam but with γ held fixed at 12 and ℓ varied from 1 to 20. Again, agreement between theory and simulation is excellent. The few simulations in Fig. 7 performed with rigid disks instead of discrete particles further vindicate the rigid disk approximation made in our model.

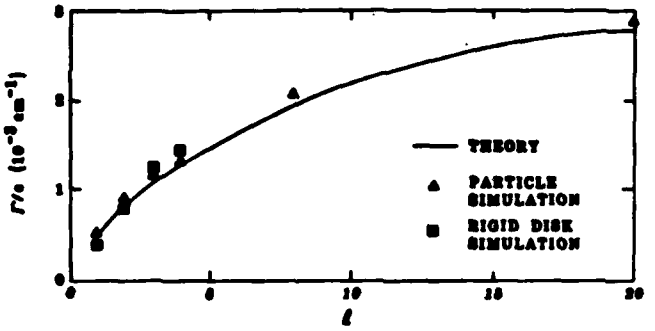

Figure 7. Negative mass growth rates at various ℓ for a 10 kA beam in a 1 kG guide field.

References

* Research supported by the U. S. Office of Naval Research.

[1]. P. Sprangle, C. A. Kapetanakos, and S. J. Marsh, in Proc. Fourth Intl. Conf. on High Power Electron and Ion Beams (Palaiseau, 1981).

[2]. G. Barak and N. Rostoker, Phys. Fluids 26, 856 (1983).

[3]. C. W. Roberson, A. Mondelli and D. Chernin, Phys. Rev. Lett. 50, 507 (1983).

[4]. S. Humphries and D. M. Woodall, Bull. Am. Phys. Soc. 28, 1054 (1983).

[5]. D. Chernin, A. Mondelli, and C. W. Roberson, Phys. Fluids 27, 2378 (1984).

[6]. C. A. Kapetanakos, P. Sprangle, S. J. Marsh, D. Dialetis, C. Agritellis, and A. Prakash, "Rapid Electron Beam Accelerators," NRL-5503 (Naval Research Lab., Washington, 1985).

[7]. A. Faltens, G. R. Lambertson, J. M. Peterson and J. B. Rechen, in Proc. IXth Intl. Conf. on High Energy Accelerators (Stanford University, 1974).

[8]. P. Sprangle and J. L. Vomvoridis, "Longitudinal and Transverse Instabilities in a High Currents Modified Betatron Electron Accelerator," NRL-4688 (Naval Research Lab., Washington, 1982).

[9]. B. B. Godfrey and T. P. Hughes, Phys. Fluids 28, 669 (1985).

[10]. T. P. Hughes and B. B. Godfrey, "Modified Betatron Accelerator Studies," AMRC-R-655 Mission Research Corp., Albuquerque, 1984).

[11]. T. P. Hughes and B. B. Godfrey, Appl. Phys. Lett. 46, 473 (1985).

[12]. V. K. Neil and A. M. Sessler, Rev. Sci. Instr. 36, 429 (1965).

[13]. R. M. Landau, Phys. Fluids 11, 205 (1968).

END

FILMED

9-85

DTIC